JACS
JOURNAL OF THE AMERICAN CHEMICAL SOCIETY
pubs.acs.org/JACS
Article

One-Pot Cyclization to Large Peptidomimetic Macrocycles by In Situ-Generated β-Turn-Enforced Folding

Fei Gou, Di Shi, Bohan Kou, Zhao Li, Xiaosheng Yan, Xin Wu, and Yun-Bao Jiang*

Cite This: J. Am. Chem. Soc. 2023, 145, 9530−9539
Read Online

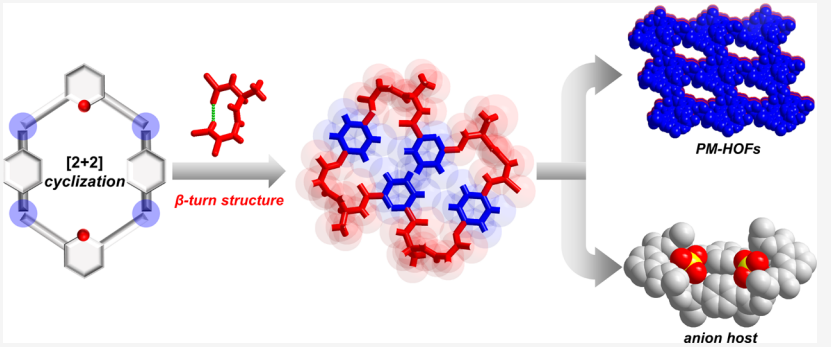

ABSTRACT: Macrocycles have been targets of extensive synthetic efforts for decades because of their potent molecular recognition and self-assembly capabilities. Yet, efficient syntheses of macrocyclic molecules via irreversible covalent bonds remain challenging. Here, we report an efficient approach to large peptidomimetic macrocycles by using the in situ-generated β-turn structural motifs afforded in the amidothiourea moieties from the early steps of the reaction of 2 molecules of bilateral amino acid-based acylhydrazine with 2 molecules of diisothiocyanate. Four chiral and achiral peptidomimetic large macrocycles were successfully synthesized in high yields of 45−63% in a feasible one-pot reaction under sub-molar concentration conditions and were purified by simple filtration. X-ray crystallographic characterization of three macrocycles reveals an important feature that their four β-turn structures, each maintained by four 10-membered intramolecular hydrogen bonds, alternatively network the four aromatic arms. This affords an interesting conformation switching mode upon anion binding. Binding of SO_4^{2-} to **1L** or **1D** that contains 4 alanine residues (with the lowest steric hinderance among the macrocycles) leads to an inside-out structural change of the host macrocycle, as confirmed by the X-ray crystal structure of **1L**-SO_4^{2-} and **1D**-SO_4^{2-} complexes, accompanied by an inversion of the CD signals. On the basis of the strong sulfate affinity of the macrocycles, we succeeded in the removal of sulfate anions from water via a macrocycle-mediated liquid−liquid extraction method. Our synthetic protocol can be easily extended to other macrocycles of varying arms and/or chiral amino acid residues; thus, a variety of structurally and functionally diverse macrocycles are expected to be readily made.

INTRODUCTION

Macrocycles continue to be the subject of extensive investigations in supramolecular, material, and biomedical chemistry, partly because of their function as host frameworks.[1−13] Despite a number of pioneering studies in the last two decades,[14−26] efficient approaches to the design and syntheses of macrocycles remain challenging. Because of the entropic cost in almost all macrocyclization reactions, the major challenges are the low yields and the formation of many byproducts requiring tedious purifications.[22,27,28] Thus, for macrocyclization reactions, the solution is made extremely dilute to avoid undesired polymerization reactions.[29] To increase the reaction efficiency, a well-established strategy is the conformational pre-organization of the reaction precursor, which can be categorized into two approaches: external auxiliary (template) and conformational regulation via intramolecular interactions.[27] The former is exemplified in the synthesis of crown ether in which the binding of the alkaline metal cation to the oxygen atoms in the precursor molecule brings the two reactive groups into close proximity [Figure 1a(i)].[30,31] For the latter approach, it is known that the installation of a turn unit mimicking those found in protein secondary structures can fold a linear precursor and thereby direct the two reacting groups at the two termini of the precursor into proximity to facilitate the cyclization.[27,32,33] For

Received: November 3, 2022
Published: April 10, 2023

https://doi.org/10.1021/jacs.2c11684
J. Am. Chem. Soc. 2023, 145, 9530−9539

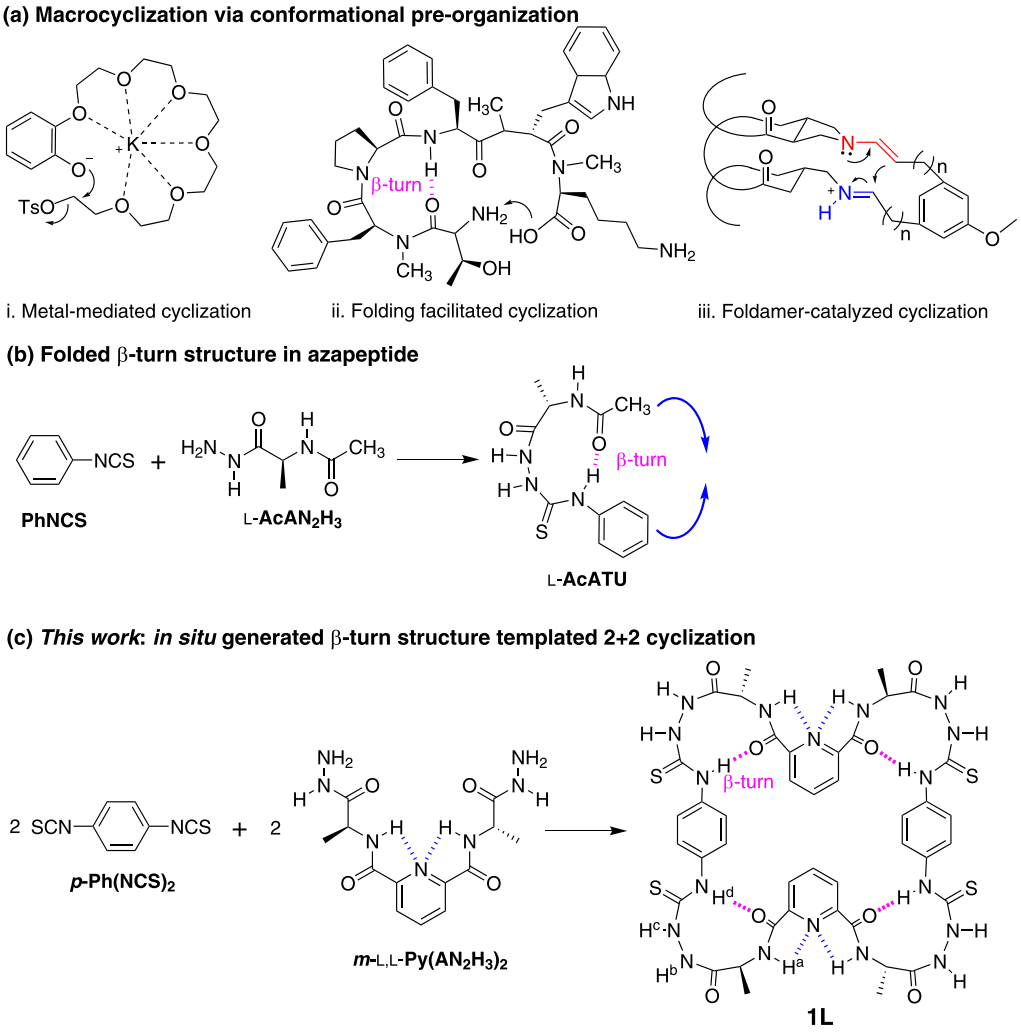

Figure 1. (a) Template-mediated cyclization strategies and (b) reaction of phenylisothiocyanate and *N*-acetylalanine hydrazine leading to amidothiourea that contains a *β*-turn structure bringing its two termini into close proximity. (c) This work: *β*-turn-mediated "2 + 2" macrocyclization leading to 46-membered large macrocycle **1L**.

example, the benzanilide-based structural motif bearing an *o*-methoxy group in the benzoyl and/or aniline moiety adopts a folded conformation because of the intramolecular hydrogen bonding between the methoxy O atom and the amide −NH proton, promoting the cyclization reaction that produces rigid macrocycles.[34−38] The *β*-turn structure was reported to facilitate the syntheses of cyclic peptides [Figure 1a(ii)].[39−42] The $^{\delta}$Orn turn unit, a *β*-turn mimic exploited by Nowick et al., was found applicable for constructing the macrocyclic *β*-hairpin peptides.[43−45] The dimethoxy cyclohexadiene motif developed by Jasti and Bertozzi has been used to synthesize carbon nanohoops.[46−48] Recently, Gellman et al.[49] used an aromatic foldamer to catalyze the macrocyclization of flexible linear dialdehyde substrates by aldol condensation [Figure 1a(iii)].

Reported herein is a novel approach applied in a conformationally controlled "2 + 2" reaction that leads to large macrocycles. This is inspired by our discovery of the *β*-turn structure formed in the product of the reaction between acylamino acid-based acylhydrazine and phenylisothiocyanate (Figure 1b).[50,51] In the amidothiourea motif, the formed hydrogen bond brings the two terminal acetyl groups and the phenyl group into close proximity. This is expected to function as a folding unit to promote the cyclization. We therefore propose to build peptidomimetic macrocycles using the corresponding bilateral reactants to allow a "2 + 2" cyclization reaction, assuming that the intermediates generated during the reaction are preorganized by their own *β*-turn structures, forming a dominant folded conformation to facilitate the cyclization reaction, eventually leading to the macrocycle containing four *β*-turn structures with 4 amino acid residues in total (Figure 1c). We have succeeded in obtaining 46-membered large macrocycles **1L**/**1D**, **2L**, and **3** in high yields from acylhydrazines derived from L-/D-alanine, L-phenylalanine, and 2-amino-*iso*-butyric acid (Aib) (Figures 1c and 2a), involving the formation of four *β*-turn structures and 4 covalent bonds during the cyclization reaction, representing an efficient approach to rapid macrocycle synthesis. The obtained macrocycles exhibit interesting conformational and host−guest properties. For example, the four aromatic arms are networked by the intramolecular hydrogen bonds that maintain the *β*-turn structures. Within the cyclic backbone, the thiourea moiety is

https://doi.org/10.1021/jacs.2c11684
J. Am. Chem. Soc. 2023, 145, 9530−9539

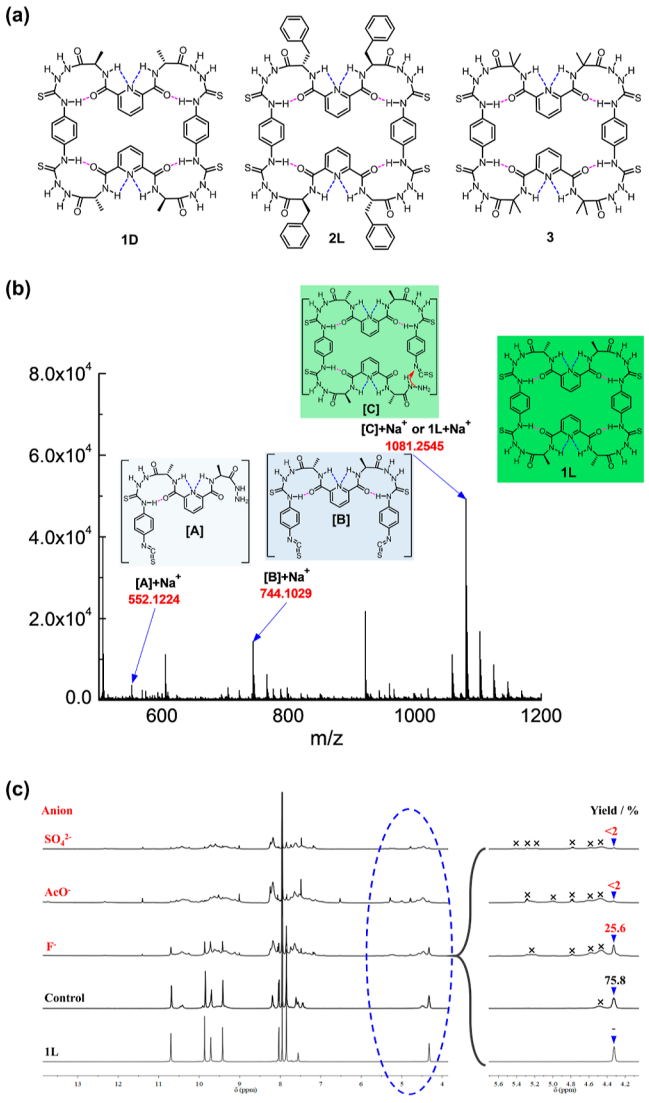

Figure 2. (a) Molecular structures of **1D**, **2L**, and **3**. (b) HRMS spectrum of the reaction mixture for the synthesis of **1L** after 10 min. (c) 600 MHz ^{1}H NMR spectra in DMSO-d_6 at 298 K from the synthesis of **1L** in the presence of 1 equiv of the given anion carried out in 1:1 (v/v) CH_3CN/DMF at 90 °C for 24 h. The presented yield of the synthesis was calculated by calculating the percentage of the NMR signal at 4.3 ppm from the chiral CH proton of **1L** over the total signals from all species containing that chiral CH proton. For comparison, the NMR spectrum of **1L** is also given. Anions are used as Bu_4N^+ salts.

known to bind anions,[52,53] such that it would undergo a local structural change to afford the required cis-conformation, leading to possibly an allosteric effect. This is confirmed in the case of binding SO_4^{2-} by the crystal structure of the **1L**-SO_4^{2-} or **1D**-SO_4^{2-} complex, which shows an inside-out structural switch of the macrocyclic host molecule. More importantly, this macrocycle has also been successfully applied to extract SO_4^{2-} from water to an organic solvent, showing promising application in water purification and industrial wastewater treatment.

RESULTS AND DISCUSSION

Syntheses of "2 + 2" Macrocycles. Our recent success in the efficient synthesis of a macrocycle from a "1 + 1" reaction of 1 molecule of *m*-Ph(CONHCH(CH_3)C(O)$NHNH_2$)$_2$ and 1 molecule of *m*-Ph(NCS)$_2$ (Figure S1a)[54] has encouraged us to explore more challenging macrocycle syntheses, since it suggests that the β-turn structure in the generated amidothiourea motif may have promoted the cyclization. Note that in those reactant molecules, the reactive groups are meta-substituted on the phenyl arms. The para-substituted reactants, at least one of the two, were therefore expected to lead to macrocycles of larger sizes, if in situ-generated β-turn structure can promote the cyclization (Figure S1b). We thus proposed to explore the "2 + 2" cyclization reactions between 2 molecules of *para*-benzenediisothiocyanate and 2 molecules of pyridine *meta*-substituted diacylhydrazine (Figure 1c).

The syntheses were found to be high yielding (Table S1 for **1L**). Under the optimized solvent condition of 1:1 (v/v) DMF/CH_3CN, the "2 + 2" macrocyclization product **1L** was obtained in a 63% isolated yield at a sub-molar concentration condition, after simply a direct filtration with no need for further purification (Figure S2). The formation of the 46-membered large macrocycle involves the formation of 4 covalent bonds (Figure 1c). The 3 other macrocyclic molecules, D-alanine-based **1D**, L-phenylalanine-based **2L**, and achiral Aib-based **3**, were similarly obtained (Figure 2a), in yields of 60, 45, and 56%, respectively, from the corresponding acylhydrazine starting materials (Scheme S1). They were fully characterized by ^{1}H NMR, ^{13}C NMR, and electrospray ionization−high-resolution mass spectroscopy (HRMS), while **1L** was further characterized by DOSY (Figure S3) and 2D COSY/NOESY/ROESY (Figure S4). The structures of three of them, **1L**, **1D**, and **3**, were confirmed by X-ray single-crystal diffraction (see the Supporting Information for details). ^{1}H NMR was first employed to examine if the expected β-turn is formed within **1L**, as an example, in the solution phase. All protons were assigned by 2D COSY/NOESY/ROESY spectra in 9:1 (v/v) CD_3CN/DMSO-d_6 (Figure S4). The β-turn structure in **1L** was indicated by ^{1}H NMR traces in CD_3CN/DMSO-d_6 binary solvents of increasing composition of the competitive DMSO-d_6, which shows only minor changes in the resonance of the thioureido −NH^d proton (Figures S5 and S6). This indicates that the thioureido −NH is involved in an intramolecular hydrogen bond.[55] Meanwhile, the change in the chemical shift of −NH^a was also found to be minor, supporting its involvement in an intramolecular hydrogen bonding with the pyridine N atom.[56−60] The temperature coefficients of the chemical shifts of −NH^d and −NH^a protons ($\Delta\delta/\Delta T$ = −1.8 and −5.4 ppb/K, respectively) are smaller than those of −NH^c (−10.9) and −NH^b (−8.8), again supporting their involvement in intramolecular hydrogen bonding (Figures S7 and S8).[61]

In order to clarify the process and mechanism of the cyclization reaction, first, HRMS spectra of the reaction mixtures were taken 10, 20, 30, 40 and 50 min and 1 h, 2 h, 3 h, and 4 h into the reaction (Figures 2b and S9 and S10). White precipitates, identified as the final product, were observed at 1 h, and more precipitates formed with longer reaction time. The HRMS spectrum of the reaction mixture 10 min after the reaction indicates the presence of not only the **A** + Na^+ ion (**A** represents the intermediate with one β-turn structure) but also the **B** + Na^+ species (**B** represents the intermediate containing two β-turn structures). The **C** + Na^+ species (**C** represents the intermediate containing three β-turn structures) may exist, but this could not be confirmed as the molecular weight of **C** is identical to that of the final product

https://doi.org/10.1021/jacs.2c11684
J. Am. Chem. Soc. 2023, 145, 9530−9539

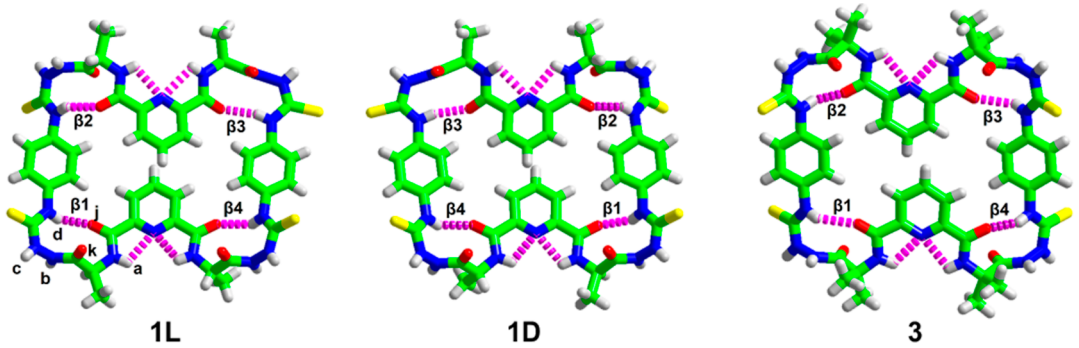

Figure 3. Crystal structures of **1L**, **1D**, and **3**. Note that the crystal structures of **1L** and **1D** from L- and D-alanine residues, respectively, are mirror-imaged.

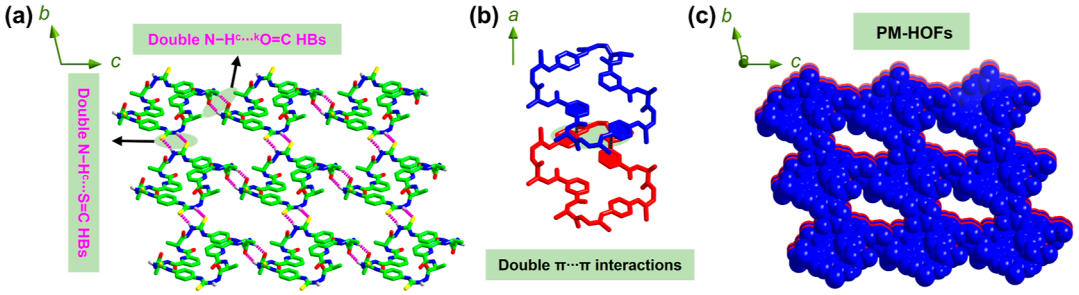

Figure 4. (a) 2D supramolecular layer structure of **1L** along the *bc* plane, formed via double N−H^{c}···^{k}O═C hydrogen bonds along the *c*-axis and double N−H^{c}···S═C hydrogen bonds along the *a*-axis. (b) Double $\pi\cdots\pi$ interactions between **1L** molecules along the *a*-axis. (c) 3D supramolecular porous structure of **1L** viewed along the *a*-axis. Except for the hydrogen atoms involved in the formation of hydrogen bonds, other H-atoms are omitted for clarity.

(**1L**). With the lengthening of the reaction duration in the early stage, the amounts of species of lower m/z decrease, while the final product becomes increasingly dominant (Figure S9), until eventually it is almost the sole component at the later stage of the reaction (Figure S10). The HRMS data thus suggest that the final macrocyclic product **1L** is formed in a stepwise manner (Figure S1b). We also monitored the NMR and HPLC of the reaction solution during the course and indeed found evidence of the quick generation of the intermediates together with the final product and the subsequent conversion of the intermediates into the product (Figures S11 and S12).

The next experiment to demonstrate the key role of the in situ-generated β-turns is the synthesis in the presence of anions such as AcO^-, F^-, or SO_4^{2-} that binds to the thiourea moiety in the turn structure (Table S2 for **1L**). The anion binds to the thiourea moiety and was expected to break the turn structure and thereby disrupt the folding-mediated macrocyclization. NMR data show that in the presence of 1 equiv of F^-, AcO^-, or SO_4^{2-} the reaction yields for **1L** drop dramatically (Figure 2c), from 75.8 to 25.6% (F^-) and to less than 2% (AcO^- and SO_4^{2-}). Detailed investigations show that with increasing concentration of AcO^- at 0, 0.1, 0.3, 0.5, and 1 equiv, the yield drops from 75.8 to 71.4, 62.9, 27.5, and 2%, respectively (Figure S13).

Crystal Structures. High-quality colorless single crystals of 3 of the 4 macrocycles, **1L**, **1D**, and **3**, suitable for X-ray single-crystal diffraction, were obtained by slow vapor diffusion of isopropyl ether into DMF solutions of the macrocyclic compounds within 7 days. The crystal structures of them, shown in Figure 3, indicate that **1L** and **1D** crystallize in the *P*1 space group as mirror images to each other, while **3** crystallizes in the $P\bar{1}$ space group (for crystallographic data, see Table S3). All of these macrocyclic molecules are oblong-shaped, each containing four β-turn structures, i.e., β1, β2, β3, and β4 (Figure 3), of two types, β-II and β-II′ (Table S4).[62] The crystal structures confirm the existence of four β-turn structures that are maintained by the 10-membered intramolecular hydrogen bonds, which network the four aromatic arms. The high yields of the syntheses are thus attributed to the final product molecule being networked by the four turn structures, which could have generated cooperativity during the cyclization process. This networking also strengthens the intramolecular hydrogen bonds that maintain the turn structure, as supported by the sluggish changes in the chemical shift of the $-NH^d$ proton of **1L** upon heating its CD_3CN/DMSO-d_6 mixtures or increasing the component of DMSO-d_6 in CD_3CN (Figures S5−S8), compared with the observation from a corresponding acyclic counterpart containing only one β-turn.[51]

Interestingly, the macrocyclic molecules **1** and **3** were found to form a unique type of peptidyl macrocyclic hydrogen-bonded organic frameworks (PM-HOFs, Figure 4). Along the *c*-axis, adjacent **1L** molecules are linked via double N−H^{c}···^{k}O═C hydrogen bonds, while along the *b*-axis, double N−H^{c}···S═C hydrogen bonds bridge the macrocycles into a 2D supramolecular layer within the *bc* plane (Figure 4a). The 2D layers stack along the *a*-axis via double $\pi\cdots\pi$ interactions (Figure 4b), resulting in a 3D-supramolecular structure (Figure 4c). Both the *bc* plane (Figure 4c) and *ab* plane are porous (Figure S14a), while the *ac* plane is filled fully (Figure S14b), affording a porous 3D-supramolecular structure with 2D channels of pore sizes of 14.2 Å × 13.5 Å and 13.9 Å × 8.2 Å (Figure S15). The stacking and bonding modes in the

https://doi.org/10.1021/jacs.2c11684
J. Am. Chem. Soc. 2023, 145, 9530−9539

crystals of **1D** (Figure S16) are exactly the same as those in **1L**, while the macrocyclic structures, 2D supramolecular layers, and 3D porous structures of **1L** and **1D** are mirror-imaged (Figure S17). To the best of our knowledge, these are the first examples of chiral PM-HOFs. With achiral macrocycle **3**, similar 3D porous supramolecular structures with 2D channels are identified too (Figure S18). The pore sizes, 16.9 Å × 14.9 Å and 14.3 Å × 9.3 Å in **3** (Figure S19), are larger than those of **1L** and **1D**, probably because of the differences in the hydrogen bonds that maintain the pore structures (Table S5).

It is noteworthy that, despite the difficulty in obtaining large quantities of single crystals from most of the reported peptide-related macrocycles,[63,64] our peptidomimetic macrocycles, **1L**, **1D**, and **3**, were found to easily crystallize such that a large quantity of blocky and needle crystals of **1L** and **1D** could be obtained in a high yield of 80% in the CH_3OH–DMF mixed solvent in only 1 day (Figure S20). This provides an interesting type of polymeric porous materials of the HOF that has hitherto been reported mostly from rigid molecular building blocks.[65−67] These first examples of PM-HOFs may in the future find their applications as functional porous crystalline materials.

Anion Binding. A distinct structural character of these macrocyclic molecules is that the four β-turn structures along the cyclic backbone are networked. A local structural change with one β-turn structure would likely lead to a dramatic change in the total macrocyclic backbone. This is expected to occur when anions bind to the thiourea motif within the β-turn structure, since the thiourea moiety in the turn structure exists in its cis,trans-conformation but not the required trans,trans-conformation for anion binding.[51,68−70] Anion binding by macrocycles **1**−**3** of increasing steric hindrance imposed by the amino acid residues were therefore evaluated and compared. Anion binding by **1L** or **1D** was first examined by absorption and CD spectroscopic titrations. **1L** and **1D** exhibit mirror-imaged CD spectra in 99.5:0.5 (v/v) CH_3CN/DMSO (Figure 5), showing three Cotton effects at 250, 268, and 295 nm with

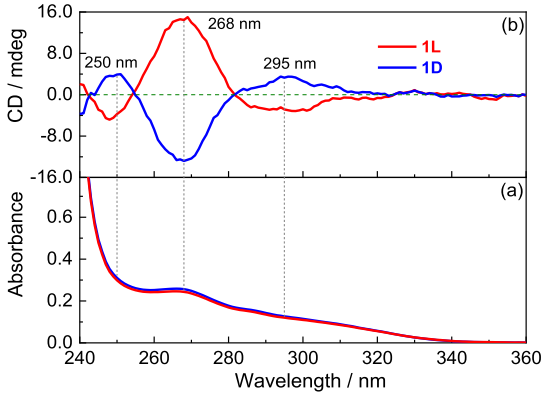

Figure 5. Absorption (a) and CD (b) spectra of **1L** and **1D** in 99.5:0.5 (v/v) CH_3CN/DMSO mixtures. [**1L**] = [**1D**] = 5 μM.

a high anisotropic factor g of 1.7×10^{-3} at 268 nm (Figure S21). A linear concentration dependence of the CD signal of **1L** over 0.2−10 μM in CH_3CN/DMSO suggests that it exists in its monomeric form (Figure S22).

CD spectra of **1L** at 5 μM in 99.5:0.5 (v/v) CH_3CN/DMSO in the presence of 10 equiv of individual anions, F^-, Cl^-, Br^-, I^-, OH^-, NO_3^-, ClO_4^-, BF_4^-, AcO^-, $H_2PO_4^-$, HCO_3^-, or SO_4^{2-} (Figure 6a,b) show that SO_4^{2-} causes the most drastic change in the CD spectrum, by reversing the sign and eventually leading to an amplified signal (g factor -3.6×10^{-3} of SO_4^{2-}/**1L** at 268 nm vs 1.7×10^{-3} of **1L**, Figure S23), and $H_2PO_4^-$ leads to a similar yet moderate response in the CD spectra, whereas the remaining anions including F^-, AcO^-, and OH^- result in opposite and minor or no changes in the spectra (Figure 6b). The profiles shown in Figure 6b therefore suggest that the spectral changes do not simply result from anion binding to the thiourea moieties, since the much stronger changes induced by multidentate SO_4^{2-} and $H_2PO_4^-$ suggest a chelating effect.[52] Detailed CD spectral titrations of **1L** by SO_4^{2-} show first a gradual inversion of the CD signals originally at 250, 268, and 295 nm and later enhancements of the signals, with two isosbestic points (Figure 6c). This means a stoichiometric binding takes place between SO_4^{2-} and **1L** up to 2 equiv of the anion. Job plots suggest a 1:2 (**1L**/SO_4^{2-}) binding stoichiometry (Figure S24) which was confirmed in the structure of the obtained bis-sulfate complex by X-ray crystallography, as described later. The SO_4^{2-}/**1L** binding constant in 99.5:0.5 (v/v) CH_3CN/DMSO was estimated to be extremely high with large errors; we therefore suggest a lower limit of 10^7 M^{-1} for K_1 (Figure S25a), while the sigmoidal binding isotherm suggests a cooperative CD response from two SO_4^{2-} anions flipping the conformation of the macrocyclic host molecule.[71,72] Moving to 100% DMSO as a more competitive solvent condition, SO_4^{2-} binding was found weakened (Figures S26 and S27), which allows a credible fitting of the binding constant giving $K_1 = 5.05 \times 10^6$ M^{-1} and $K_2 = 1.24 \times 10^4$ M^{-1} (Figure S25b). Titrations by other anions, F^-, AcO^-, $H_2PO_4^-$, and OH^-, exhibited diverse response profiles (Figures S28−S31). We attempted to determine the binding constants of these ions but, except the AcO^-, found the equilibria complicated by the occurrence of the anion-induced deprotonation of the NH groups in **1L**, to different extents, as shown in the ^1H NMR spectral traces (Figure S32), despite the occurrence of anion binding at low anion concentrations. The binding constant for complexation of **1L** with AcO^- was also too high to be accurately determined in 99.5:0.5 (v/v) CH_3CN/DMSO (Figures S32d and S34a). We therefore also examined AcO^- binding in 100% DMSO, which allows a credible fitting of the binding constant, giving $K_1 = 4.53 \times 10^6$ M^{-1} and $K_2 = 7.80 \times 10^3$ M^{-1} (Figures S33 and S34b). Although K_1 for AcO^- is only slightly lower than that for SO_4^{2-} in pure DMSO, **1L** exhibits a significant selectivity for SO_4^{2-} over AcO^- in 99.5:0.5 (v/v) CH_3CN/DMSO (shown by a competition experiment, Figure S36) because the lower polarity of CH_3CN medium favors the binding of doubly charged SO_4^{2-}.

To further show the selective binding of SO_4^{2-} with **1L**, we examined the absorption and CD spectral response of **1L** toward multivalent anions, $S_2O_8^{2-}$, HPO_4^{2-}, p-$Ph(CO_2)_2^{2-}$, $C_2O_4^{2-}$, $-O_2C(CH_2)_2CO_2^{2-}$, and PO_4^{3-} (Figure S35). These anions, except $S_2O_8^{2-}$, resulted in varying extents of spectral responses but are much less than that induced by SO_4^{2-} (Figure 6b), supporting the high selectivity for SO_4^{2-} binding by **1L**. Competitive experiments showed that the CD response of **1L** induced by SO_4^{2-} is not affected by the presence of most tested anions (Figures S36 and S37), again indicating a high selectivity of the macrocyclic host **1L** for SO_4^{2-}. Significant interference of SO_4^{2-} binding was observed for highly basic anions, such as OH^-, HPO_4^{2-}, and PO_4^{3-}, likely due to these anions deprotonating **1L**.

https://doi.org/10.1021/jacs.2c11684
J. Am. Chem. Soc. 2023, 145, 9530−9539

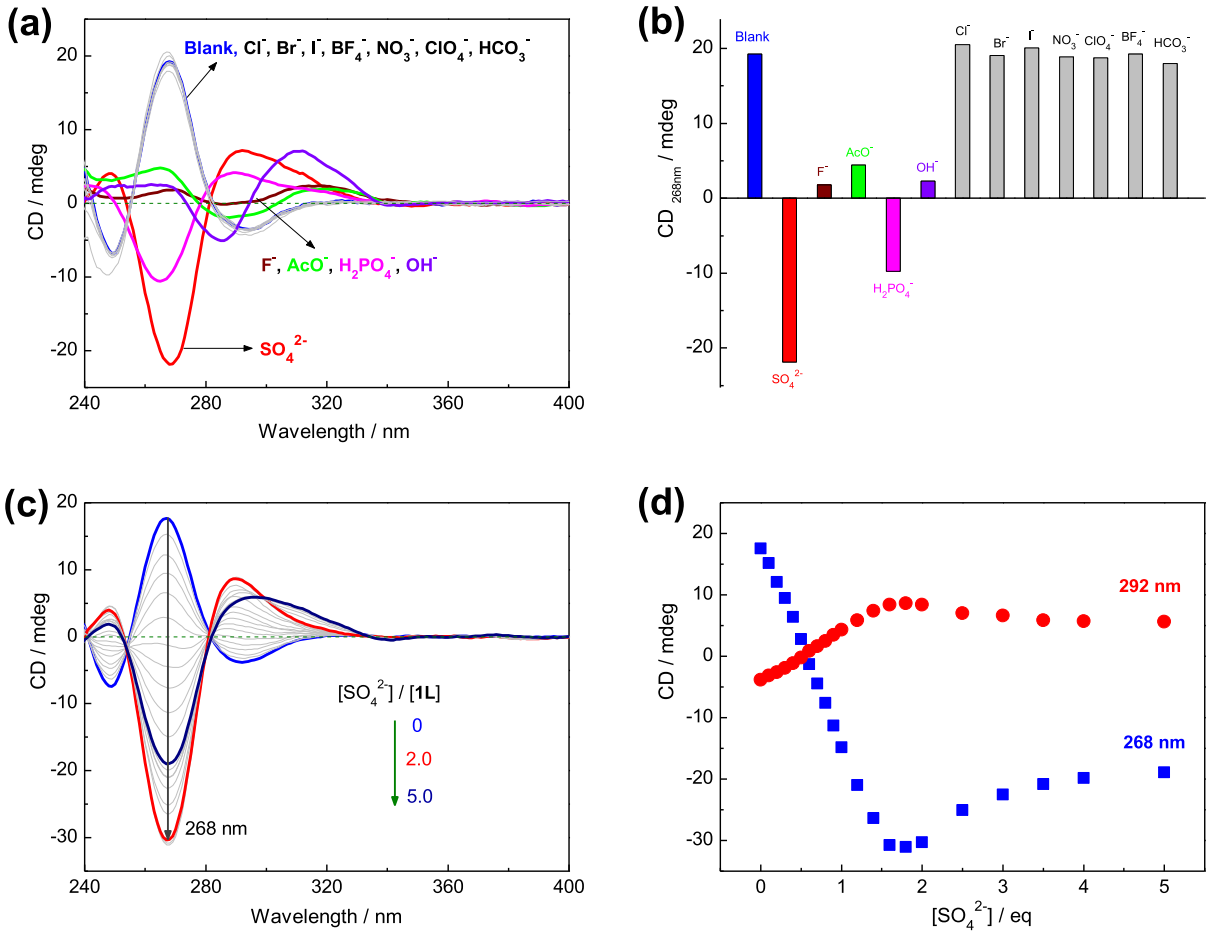

Figure 6. (a) CD spectra and (b) histogram of the CD signal of **1L** at 268 nm in 99.5:0.5 (v/v) CH_3CN/DMSO in the presence of 10 equiv of the tested anion. (c) CD spectra in 99.5:0.5 (v/v) CH_3CN/DMSO in the presence of SO_4^{2-} from 0 to 5 equiv and (d) plots of CD signals of **1L** at 268 and 294 nm vs concentration of SO_4^{2-}. [**1L**] = 5 μM. All anions exist in their *n*-Bu_4N^+ (TBA^+) salts.

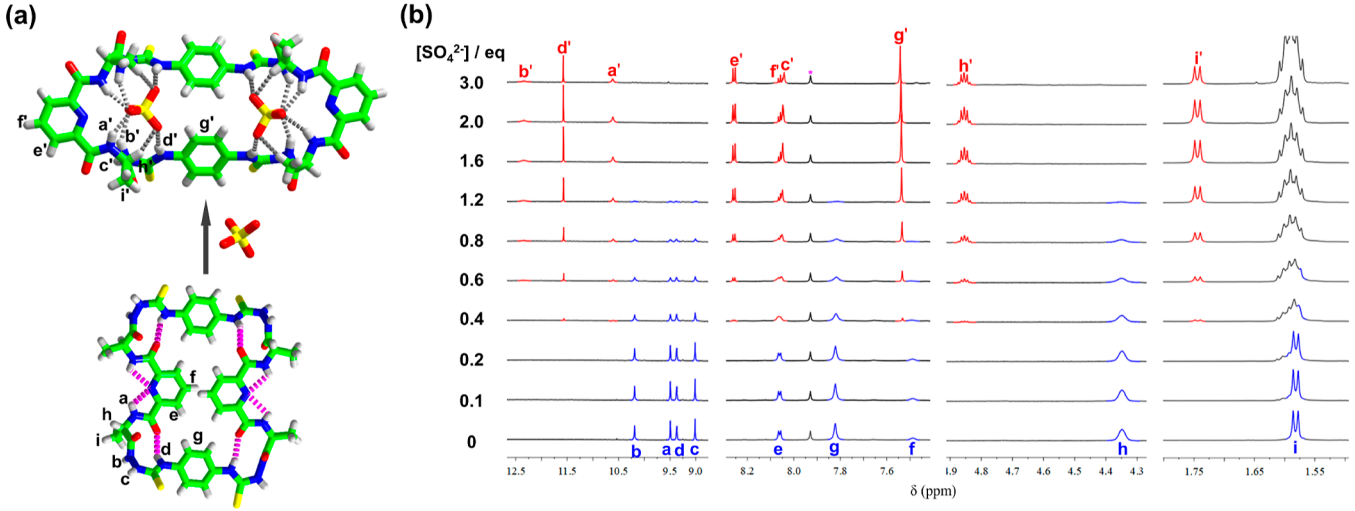

Figure 7. (a) X-ray crystal structure of the $[\mathbf{1L}\cdot(SO_4)_2]^{4-}$ complex. TBA^+ countercations are omitted for clarity. (b) Partial 850 MHz ^1H NMR spectra of **1L** upon titration by SO_4^{2-} in 9:1 (v/v) CD_3CN/DMSO-d_6 at 298 K. [**1L**] = 0.1 mM, TBA^+ salt of the sulfate anion was used.

Absorption and CD spectra of **2L** and absorption spectra of **3** at 5 μM in 99.5:0.5 (v/v) CH_3CN/DMSO were next examined in the presence of 10 equiv of SO_4^{2-} and the above monovalent anion (Figures S38−S43). It was found that the response profiles in the absorption spectra of **1**−**3** toward those anions appear similar (Figures S30b, S40b and S42b), where more pronounced responses were observed for SO_4^{2-}, F^-, AcO^-, $H_2PO_4^-$ and OH^-. An exception is that the absorption spectra of **3** showed weak responses to $H_2PO_4^-$ (Figures S42 and S43c). We also found that the changes of the CD spectra of **2L** induced by all those anions such as SO_4^{2-}, F^-, AcO^-, $H_2PO_4^-$, and OH^- are similar (Figure S38), differing from that

https://doi.org/10.1021/jacs.2c11684
J. Am. Chem. Soc. 2023, 145, 9530−9539

observed for **1L** (Figure 6b). This means that a conformation change may have not occurred in **2L** upon its binding to those anions. Together with the much weaker response of the absorption spectrum of **3** toward $H_2PO_4^-$, we assume that the increasing steric hindrance in the order **1L** < **2L** < **3** prevents the conformation change of the macrocyclic host molecules in the latter cases. We also examined the spectral responses of **2L** or **3** toward the tested multivalent anions (Figure S44). Again, the response profiles are similar to those of **1L** (Figure S35a).

Our success in growing the colorless crystal of the SO_4^{2-}/**1L** binding complex, by slow diffusion of isopropyl ether into DMSO solution of **1L** within one month, allows X-ray crystallographic characterization (for crystallographic data, see Supporting Information, Table S6), which indicates that the crystal is of space group $P2_12_12$, with a boat-like conformation of the macrocycle in a 1:2 stoichiometry (Figures 7a and S45a). Two SO_4^{2-} anions are each held at the two pockets within the macrocycle, via six N−H···O and two C−H···O hydrogen bonds (H···O distances ranging from 1.942 to 2.596 Å and X−H···O angles ranging from 128 to 163°; Figure 7a and Table S7), while four *n*-Bu_4N^+ countercations are located outside the macrocycles to balance the charges (Figure S45b). In the complex, each SO_4^{2-} anion interacts with two β-turn structures, leading to the breaking of the 10-membered ring hydrogen bonds to form a new C_2 symmetric structure. Indeed, the conformation of the macrocyclic host itself inverts such that almost all of the outward N−H protons point inward to coordinate with the SO_4^{2-} anions, while the pyridine groups flip inside out. Interestingly, a double-helix-like structure was identified along the *a*-axis of the crystal of the complexes, in which almost 2 complex molecules form a repeating unit (Figure S46). The $N-H^{c}\cdots{}^{j}O{=}C$ hydrogen bonding and $\pi-\pi$ stacking link the repeating units into two helical strands, while SO_4^{2-} anions intertwine the two strands. The crystal structure of the complex of SO_4^{2-} with **1D** (Figure S47), the enantiomer of **1L**, is mirror-imaged to that of the SO_4^{2-}/**1L** complex, with exactly the same stacking and bonding modes.

In view of this dramatic change in the molecular structure of the host molecule of **1L** or **1D** upon SO_4^{2-} binding, a substantial change in the ^{1}H NMR was expected, and it was experimentally verified (Figure 7). Traces of ^{1}H NMR of **1L** in 9:1 (v/v) CD_3CN/DMSO-d_6 in the presence of increasing concentration of SO_4^{2-} show an upfield shift of the signal of the $-NH^c$ proton ($\Delta\delta$ = 0.97 ppm), while those of the remaining three −NH protons undergo significant downfield shifts ($\Delta\delta$ = 1.25−2.16 ppm), suggesting that SO_4^{2-} anions are tightly bound with −NH protons of **1L** (Figure 7b). In particular, new sets of signals appear with $-CH_3$ protons (1.74 ppm), chiral −CH proton (4.85 ppm), phenyl protons (7.53 ppm), and pyridine protons (8.06 and 8.26 ppm), evident of a slow-exchange complexation and the high stability of the complex. 2D NMR experiments on **1L** and the $[\mathbf{1L}\cdot(SO_4)_2]^{4-}$ complex were performed to help clarify the structure of the complex. For **1L**, obvious ROE and NOE peaks between hydrogen atoms on phenyl and pyridine groups (CH^e and CH^g, 2.550 Å) were observed, but not for NH^a-NH^b (4.358 Å), agreeing with their distances identified in the crystal structure (Figure S4). While for the $[\mathbf{1L}\cdot(SO_4)_2]^{4-}$ complex, the ROE and NOE peaks of $NH^{a'}-NH^{b'}$ (2.676 Å) were observed, but not for the $CH^{e'}-CH^{g'}$ (9.487 Å) (Figure S48). These again support the structural inversion of the macrocyclic host upon binding to SO_4^{2-} anions. Diffusion ordered spectroscopy (DOSY) of **1L** and the $[\mathbf{1L}\cdot(SO_4)_2]^{4-}$ complex at 298 K led to the diffusion coefficient of **1L** of 1.06×10^{-10} m^2 s^{-1} and of the $[\mathbf{1L}\cdot(SO_4)_2]^{4-}$ complex of 1.00×10^{-10} m^2 s^{-1}, ruling out the formation of large aggregates (Figure S49), which is also supported by the dynamic light scattering data (Figure S50).

Similar NMR titrations on **2L** and **3** show that the signals shift upon binding to SO_4^{2-} anions (Figures S51 and S52), different from that observed for **1L**, again suggesting that SO_4^{2-} binding to **2L** and **3** resulted in less structural changes, if any, as that suggested by the changes in the absorption and CD spectra. This is tentatively assigned to the increasing steric hindrance of the substituent in the amino acid residue, from $-CH_3$ (**1**) to $-CH_2Ph$ (**2**) and finally to two $-CH_3$ groups (**3**).

Given the widespread existence of SO_4^{2-} in various industrial wastewaters and its interference with vitrification of radioactive waste, methods for efficient removal of SO_4^{2-} from water have received significant interest.[73−75] Yet, simple and efficient separation of SO_4^{2-} is still challenging due to the higher hydration energy of SO_4^{2-} (−1080 kJ/mol) than other anions.[76] Liquid−liquid extraction is one of the most promising approaches for SO_4^{2-} separation in recent years, and the key is to find an efficient receptor.[77−81] Given the high affinity of macrocycles **1** for SO_4^{2-} anions, we examined the ability of **1L** to separate SO_4^{2-} anions from water. As shown in Figure S53a, an organic layer of **1L** (1 mM) in 95:5 (v/v) $CHCl_3$/DMSO with 4 equiv of A464Cl salts (a commercially available salt as the auxiliary reagent for extraction) and an aqueous solution of Na_2SO_4 (2 mM) were prepared and mixed. The extraction was completed by simply shaking for 10 s. The organic layer was analyzed by ^{1}H NMR to calculate the amount of SO_4^{2-} extracted from water. We carried out three extraction experiments and found the extraction efficiency to be 91.7, 93.4, and 94.3% (Figure S53b), showing that **1L** can efficiently extract SO_4^{2-} anions from the aqueous phase. We also examined the selectivity of SO_4^{2-} extraction in the presence of other anions (NO_3^-, Br^-, I^-, ClO_4^-, HCO_3^-, and HPO_4^{2-}) in water (Figure S54a). NO_3^-, Br^-, and ClO_4^- anions showed weak or negligible interference, the SO_4^{2-} extraction efficiency remaining >89%. Although other three anions induced varying extents of interference, the extraction efficiency was still >64% (Figure S54b), demonstrating a reasonable SO_4^{2-} selectivity even when coexisting with relatively strongly coordinating anions. These results indicate that our macrocycle host can be used as a potential SO_4^{2-} extraction agent for wastewater treatment.

CONCLUSIONS

We proposed a straightforward and effective approach to synthesizing the functional peptidomimetic macrocycles in high yields from a one-pot "2 + 2" cyclization of di(peptide amido)hydrazine and diisothiocynate under normal concentration conditions. We succeeded in obtaining the large peptidomimetic macrocycles containing 4 L- or D-alanine, L-phenylalanine, or Aib residues, in isolated yields ranging from 45 to 63%. The formed macrocycles contain four β-turn structures that network the four aromatic arms within the macrocyclic backbone, via 10-membered intramolecular hydrogen bonds afforded in the amidothiourea motifs. The presence of the acidic amido −NH protons and the thiourea moieties in the macrocyclic backbone enables anion binding that is expected to lead to a structural change. Crystal structures of

https://doi.org/10.1021/jacs.2c11684
J. Am. Chem. Soc. 2023, 145, 9530−9539

1L, **1D**, and **3** containing L-/D-alanine and Aib residues, respectively, confirm the networking by β-turns. This may have facilitated crystallization of macrocycles **1L**, **1D**, and **3**, which allows the generation of PM-HOFs. Macrocycles **1L** and **1D** exhibit unexpectedly strong and highly selective binding to SO_4^{2-} in an allosteric way that involves a structural inversion of the host macrocycles. With increasing steric hindrance of the substituent in the amino acid residue, the structural change becomes unfavorable such that **2L** and **3** do not bind to SO_4^{2-} as strongly and selectively as **1L** (**1D**) does. As the amino acid residues and the two kinds of aromatic arms within the macrocyclic backbone can be varied and/or structurally modified, a great variety of peptidomimetic macrocycles of diverse structures and functions have been obtained by this feasible and effective one-pot cyclization reaction. The unique host−guest properties of the peptidomimetic macrocycles have shown the potential practical applications in SO_4^{2-} removal from water.

■ ASSOCIATED CONTENT

Supporting Information

The Supporting Information is available free of charge at https://pubs.acs.org/doi/10.1021/jacs.2c11684.

Detailed synthetic procedures, characterization, crystal data, spectral analysis, and others (PDF)

Accession Codes

CCDC 2153163−2153167 contain the supplementary crystallographic data for this paper. These data can be obtained free of charge via www.ccdc.cam.ac.uk/data_request/cif, or by emailing data_request@ccdc.cam.ac.uk, or by contacting The Cambridge Crystallographic Data Centre, 12 Union Road, Cambridge CB2 1EZ, UK; fax: +44 1223 336033.

■ AUTHOR INFORMATION

Corresponding Author

Yun-Bao Jiang − *Department of Chemistry, College of Chemistry and Chemical Engineering, The MOE Key Laboratory of Spectrochemical Analysis and Instrumentation, and Collaborative Innovation Center of Chemistry for Energy Materials (iChEM), Xiamen University, Xiamen 361005, China;* orcid.org/0000-0001-6912-8721; Email: ybjiang@xmu.edu.cn

Authors

Fei Gou − *Department of Chemistry, College of Chemistry and Chemical Engineering, The MOE Key Laboratory of Spectrochemical Analysis and Instrumentation, and Collaborative Innovation Center of Chemistry for Energy Materials (iChEM), Xiamen University, Xiamen 361005, China;* orcid.org/0000-0003-2749-957X

Di Shi − *Department of Chemistry, College of Chemistry and Chemical Engineering, The MOE Key Laboratory of Spectrochemical Analysis and Instrumentation, and Collaborative Innovation Center of Chemistry for Energy Materials (iChEM), Xiamen University, Xiamen 361005, China*

Bohan Kou − *Department of Chemistry, College of Chemistry and Chemical Engineering, The MOE Key Laboratory of Spectrochemical Analysis and Instrumentation, and Collaborative Innovation Center of Chemistry for Energy Materials (iChEM), Xiamen University, Xiamen 361005, China*

Zhao Li − *Department of Chemistry, College of Chemistry and Chemical Engineering, The MOE Key Laboratory of Spectrochemical Analysis and Instrumentation, and Collaborative Innovation Center of Chemistry for Energy Materials (iChEM), Xiamen University, Xiamen 361005, China*

Xiaosheng Yan − *Department of Chemistry, College of Chemistry and Chemical Engineering, The MOE Key Laboratory of Spectrochemical Analysis and Instrumentation, and Collaborative Innovation Center of Chemistry for Energy Materials (iChEM), Xiamen University, Xiamen 361005, China; School of Pharmaceutical Sciences, Xiamen University, Xiamen 361102, China;* orcid.org/0000-0002-4207-9752

Xin Wu − *School of Pharmaceutical Sciences, Xiamen University, Xiamen 361102, China; School of Chemistry and Molecular Biosciences, The University of Queensland, St Lucia, Queensland 4072, Australia*

Complete contact information is available at: https://pubs.acs.org/10.1021/jacs.2c11684

Notes

The authors declare no competing financial interest.

■ ACKNOWLEDGMENTS

We greatly appreciate the support of this work by the NSF of China (grant nos. 21820102006, 91856118, and 22101240) and the Fundamental Research Funds for the Central Universities (grant nos. 20720220005 and 20720220121). X.W. acknowledges the Australian Research Council (DE220101000) for funding. We thank Zanbin Wei from the Analytical & Testing Center of Xiamen University for X-ray diffraction work and single-crystal structural analysis. Dr. Yun Liu of Peking University is thanked for useful discussion.

■ REFERENCES

(1) Lehn, J. M. Supramolecular Chemistry: Receptors, Catalysts, and Carriers. *Science* **1985**, *227*, 849−856.

(2) Gokel, G. W.; Leevy, W. M.; Weber, M. E. Crown Ethers: Sensors for Ions and Molecular Scaffolds for Materials and Biological Models. *Chem. Rev.* **2004**, *104*, 2723−2750.

(3) Lee, S.; Chen, C.-H.; Flood, A. H. A Pentagonal Cyanostar Macrocycle with Cyanostilbene CH Donors Binds Anions and Forms Dialkylphosphate [3]Rotaxanes. *Nat. Chem.* **2013**, *5*, 704−710.

(4) Shimizu, L. S.; Salpage, S. R.; Korous, A. A. Functional Materials from Self-assembled Bis-urea Macrocycles. *Acc. Chem. Res.* **2014**, *47*, 2116−2127.

(5) Crini, G. Review: A History of Cyclodextrins. *Chem. Rev.* **2014**, *114*, 10940−10975.

(6) Liu, Z.; Nalluri, S. K. M.; Stoddart, J. F. Surveying Macrocyclic Chemistry: From Flexible Crown Ethers to Rigid Cyclophanes. *Chem. Soc. Rev.* **2017**, *46*, 2459−2478.

(7) Chen, Y.; Huang, F.; Li, Z.-T.; Liu, Y. Controllable Macrocyclic Supramolecular Assemblies in Aqueous Solution. *Sci. China: Chem.* **2018**, *61*, 979−992.

(8) Kumar, R.; Sharma, A.; Singh, H.; Suating, P.; Kim, H. S.; Sunwoo, K.; Shim, I.; Gibb, B. C.; Kim, J. S. Revisiting Fluorescent Calixarenes: From Molecular Sensors to Smart Materials. *Chem. Rev.* **2019**, *119*, 9657−9721.

(9) Song, Q.; Cheng, Z.; Kariuki, M.; Hall, S. C. L.; Hill, S. K.; Rho, J. Y.; Perrier, S. Molecular Self-Assembly and Supramolecular Chemistry of Cyclic Peptides. *Chem. Rev.* **2021**, *121*, 13936−13995.

(10) Hua, B.; Shao, L.; Li, M.; Liang, H.; Huang, F. Macrocycle-Based Solid-State Supramolecular Polymers. *Acc. Chem. Res.* **2022**, *55*, 1025−1034.

(11) Jirásek, M.; Anderson, H. L.; Peeks, M. D. From Macrocycles to Quantum Rings: Does Aromaticity Have a Size Limit? *Acc. Chem. Res.* **2021**, *54*, 3241−3251.
(12) Leonhardt, E. J.; Jasti, R. Emerging Applications of Carbon Nanohoops. *Nat. Rev. Chem.* **2019**, *3*, 672−686.
(13) Zhang, Q.; Zhang, Y.-E.; Tong, S.; Wang, M.-X. Hydrocarbon Belts with Truncated Cone Structures. *J. Am. Chem. Soc.* **2020**, *142*, 1196−1199.
(14) Gallant, A. J.; MacLachlan, M. J. Ion-Induced Tubular Assembly of Conjugated Schiff-Base Macrocycles. *Angew. Chem., Int. Ed.* **2003**, *42*, 5307−5310.
(15) Zhang, W.; Moore, J. S. Arylene Ethynylene Macrocycles Prepared by Precipitation-Driven Alkyne Metathesis. *J. Am. Chem. Soc.* **2004**, *126*, 12796.
(16) Zhang, W.; Moore, J. S. Shape-Persistent Macrocycles: Structures and Synthetic Approaches from Arylene and Ethynylene Building Blocks. *Angew. Chem., Int. Ed.* **2006**, *45*, 4416−4439.
(17) Gallant, A. J.; Chong, J. H.; MacLachlan, M. J. Heptametallic Bowl-Shaped Complexes Derived from Conjugated Schiff-Base Macrocycles: Synthesis, Characterization, and X-ray Crystal Structures. *Inorg. Chem.* **2006**, *45*, 5248−5250.
(18) Hili, R.; Rai, V.; Yudin, A. K. Macrocyclization of Linear Peptides Enabled by Amphoteric Molecules. *J. Am. Chem. Soc.* **2010**, *132*, 2889−2891.
(19) Frost, J. R.; Scully, C. C. G.; Yudin, A. K. Oxadiazole Grafts in Peptide Macrocycles. *Nat. Chem.* **2016**, *8*, 1105−1111.
(20) Majewski, M. A.; Stępien, M. Bowls, Hoops, and Saddles: Synthetic Approaches to Curved Aromatic Molecules. *Angew. Chem., Int. Ed.* **2019**, *58*, 86−116.
(21) Mortensen, K. T.; Osberger, T. J.; King, T. A.; Sore, H. F.; Spring, D. R. Strategies for the Diversity-Oriented Synthesis of Macrocycles. *Chem. Rev.* **2019**, *119*, 10288−10317.
(22) Chow, H. Y.; Zhang, Y.; Matheson, E.; Li, X. Ligation Technologies for the Synthesis of Cyclic Peptides. *Chem. Rev.* **2019**, *119*, 9971−10001.
(23) Peng, S.; He, Q.; Vargas-Zúñiga, G. I.; Qin, L.; Hwang, I.; Kim, S. K.; Heo, N. J.; Lee, C.-H.; Dutta, R.; Sessler, J. L. Strapped calix[4]pyrroles: From Syntheses to Applications. *Chem. Soc. Rev.* **2020**, *49*, 865−907.
(24) Gagnon, C.; Godin, É.; Minozzi, C.; Sosoe, J.; Pochet, C.; Collins, S. K. Biocatalytic Synthesis of Planar Chiral Macrocycles. *Science* **2020**, *367*, 917−921.
(25) Chaudhry, M. T.; Akine, S.; MacLachlan, M. J. Contemporary Macrocycles for Discrete Polymetallic Complexes: Precise Control Over Structure and Function. *Chem. Soc. Rev.* **2021**, *50*, 10713−10732.
(26) Zhang, Z.-Y.; Li, C. Biphen[n]arenes: Modular Synthesis, Customizable Cavity Sizes, and Diverse Skeletons. *Acc. Chem. Res.* **2022**, *55*, 916−929.
(27) White, C. J.; Yudin, A. K. Contemporary Strategies for Peptide Macrocyclization. *Nat. Chem.* **2011**, *3*, 509−524.
(28) Gulder, T.; Baran, P. S. Strained Cyclophane Natural Products: Macrocyclization at its Limits. *Nat. Prod. Rep.* **2012**, *29*, 899−934.
(29) Marti-Centelles, V.; Pandey, M. D.; Burguete, M. I.; Luis, S. V. Macrocyclization Reactions: The Importance of Conformational, Configurational, and Template-Induced Preorganization. *Chem. Rev.* **2015**, *115*, 8736−8834.
(30) Pedersen, C. J. Macrocyclic Polyethers: Dibenzo-18-Crown-6 Polyether and Dicyclohexyl-18-Crown-6 Polyether. *Org. Synth.* **1972**, *52*, 66.
(31) Nishino, N.; Xu, M.; Mihara, H.; Fujimoto, T.; Ueno, Y.; Kumagai, H. Sequence Dependence in Solid-Phase-Synthesis-Cyclization-Cleavage for Cyclo(-Arginyl-Glycyl-Aspartyl-Phenylglycyl-). *Tetrahedron Lett.* **1992**, *33*, 1479−1482.
(32) Blankenstein, J.; Zhu, J. Conformation-Directed Macrocyclization Reactions. *Eur. J. Org. Chem.* **2005**, *2005*, 1949−1964.
(33) Jwad, R.; Weissberger, D.; Hunter, L. Strategies for Fine-Tuning the Conformations of Cyclic Peptides. *Chem. Rev.* **2020**, *120*, 9743−9789.
(34) Yuan, L. H.; Feng, W.; Yamato, K.; Sanford, A. R.; Xu, D. G.; Guo, H.; Gong, B. Highly Efficient, One-Step Macrocyclizations Assisted by the Folding and Preorganization of Precursor Oligomers. *J. Am. Chem. Soc.* **2004**, *126*, 11120−11121.
(35) Gong, B. Hollow Crescents, Helices, and Macrocycles from Enforced Folding and Folding-Assisted Macrocyclization. *Acc. Chem. Res.* **2008**, *41*, 1376−1386.
(36) Li, Z. T.; Hou, J. L.; Li, C. Peptide Mimics by Linear Arylamides: A Structural and Functional Diversity Test. *Acc. Chem. Res.* **2008**, *41*, 1343−1353.
(37) Zhang, D. W.; Zhao, X.; Hou, J. L.; Li, Z. T. Aromatic Amide Foldamers: Structures, Properties, and Functions. *Chem. Rev.* **2012**, *112*, 5271−5316.
(38) Urushibara, K.; Ferrand, Y.; Liu, Z. W.; Masu, H.; Pophristic, V.; Tanatani, A.; Huc, I. Frustrated Helicity: Joining the Diverging Ends of a Stable Aromatic Amide Helix to Form a Fluxional Macrocycle. *Angew. Chem., Int. Ed.* **2018**, *57*, 7888−7892.
(39) Pettit, G. R.; Kamano, Y.; Herald, C. L.; Fujii, Y.; Kizu, H.; Boyd, M. R.; Boettner, F. E.; Doubek, D. L.; Schmidt, J. M.; Chapuis, J. C.; Michel, C. Isolation of Dolastatins 10−15 from the Marine Mollusc. *Tetrahedron* **1993**, *49*, 9151−9170.
(40) Chatterjee, J.; Gilon, C.; Hoffman, A.; Kessler, H. N-Methylation of Peptides: A New Perspective in Medicinal Chemistry. *Acc. Chem. Res.* **2008**, *41*, 1331−1342.
(41) Chatterjee, J.; Laufer, B.; Kessler, H. Synthesis of N-Methylated Cyclic Peptides. *Nat. Protoc.* **2012**, *7*, 432−444.
(42) Appavoo, S. D.; Kaji, T.; Frost, J. R.; Scully, C. C. G.; Yudin, A. K. Development of Endocyclic Control Elements for Peptide Macrocycles. *J. Am. Chem. Soc.* **2018**, *140*, 8763−8770.
(43) Cheng, P. N.; Liu, C.; Zhao, M.; Eisenberg, D.; Nowick, J. S. Amyloid β-Sheet Mimics that Antagonize Protein Aggregation and Reduce Amyloid Toxicity. *Nat. Chem.* **2012**, *4*, 927−933.
(44) Kreutzer, A. G.; Nowick, J. S. Elucidating the Structures of Amyloid Oligomers with Macrocyclic β-Hairpin Peptides: Insights into Alzheimer's Disease and Other Amyloid Diseases. *Acc. Chem. Res.* **2018**, *51*, 706−718.
(45) Li, X.; Sabol, A. L.; Wierzbicki, M.; Salveson, P. J.; Nowick, J. S. An Improved Turn Structure for Inducing β-Hairpin Formation in Peptides. *Angew. Chem., Int. Ed. Engl.* **2021**, *60*, 22776−22782.
(46) Jasti, R.; Bhattacharjee, J.; Neaton, J. B.; Bertozzi, C. R. Synthesis, Characterization, and Theory of [9]-[12]-and [18]-Cycloparaphenylene: Carbon Nanohoop Structures. *J. Am. Chem. Soc.* **2008**, *130*, 17646−17647.
(47) Golder, M. R.; Jasti, R. Syntheses of the Smallest Carbon Nanohoops and the Emergence of Unique Physical Phenomena. *Acc. Chem. Res.* **2015**, *48*, 557−566.
(48) Darzi, E. R.; Jasti, R. The Dynamic, Size-Dependent Properties of [5]−[12]Cycloparaphenylenes. *Chem. Soc. Rev.* **2015**, *44*, 6401−6410.
(49) Girvin, Z. C.; Andrews, M. K.; Liu, X.; Gellman, S. H. Foldamer-Templated Catalysis of Macrocycle Formation. *Science* **2019**, *366*, 1528−1531.
(50) Yan, X.-S.; Wu, K.; Yuan, Y.; Zhan, Y.; Wang, J.-H.; Li, Z.; Jiang, Y.-B. β-Turn Structure in Glycinylphenylalanine Dipeptide Based *N*-Amidothioureas. *Chem. Commun.* **2013**, *49*, 8943−8945.
(51) Yan, X.-S.; Luo, H.; Zou, K.-S.; Cao, J.-L.; Li, Z.; Jiang, Y.-B. Short Azapeptides of Folded Structures in Aqueous Solutions. *ACS Omega* **2018**, *3*, 4786−4790.
(52) Li, A.-F.; Wang, J.-H.; Wang, F.; Jiang, Y.-B. Anion Complexation and Sensing Using Modified Urea and Thiourea-based Receptors. *Chem. Soc. Rev.* **2010**, *39*, 3729−3745.
(53) He, Q.; Vargas-Zúñiga, G. I.; Kim, S. H.; Kim, S. K.; Sessler, J. L. Macrocycles as Ion Pair Receptors. *Chem. Rev.* **2019**, *119*, 9753−9835.
(54) Zhao, Z.; Zhang, M.; Tang, B.; Weng, P.; Zhang, Y.; Yan, X.; Li, Z.; Jiang, Y.-B. Transmembrane Fluoride Transport by a Cyclic Azapeptide with Two β-Turns. *Front. Chem.* **2021**, *8*, 621323.

https://doi.org/10.1021/jacs.2c11684
J. Am. Chem. Soc. 2023, 145, 9530−9539

(55) Copeland, G. T.; Jarvo, E. R.; Miller, S. J. Minimal Acylase-Like Peptides.Conformational Control of Absolute Stereospecificity. *J. Org. Chem.* **1998**, *63*, 6784−6785.
(56) Chow, H. F.; Wang, G.-X. Enhanced Gelation Property Due to Intra-Molecular Hydrogen bonding in a New Series of Bis(amino acid)-Functionalized Pyridine-2,6-Dicarboxamide Organogelators. *Tetrahedron* **2007**, *63*, 7407−7418.
(57) Marlin, D. S.; Olmstead, M. M.; Mascharak, P. K. Extendedstructures Controlled by Intramolecular and Intermolecular Hydrogen Bonding: a Case Study with Pyridine-2,6-Dicarboxamide, 1,3-Benzenedicarboxamide and N,N'-Dimethyl-2,6-Pyridinedicarboxamide. *J. Mol. Struct.* **2000**, *554*, 211−223.
(58) Berl, V.; Huc, I.; Khoury, R. G.; Krische, M. J.; Lehn, J.-M. Interconversion of Single and Double Helices Formed from Synthetic Molecular Strands. *Nature* **2000**, *407*, 720−723.
(59) Garric, J.; Leger, J.-M.; Huc, I. Molecular Apple Peels. *Angew. Chem., Int. Ed. Engl.* **2005**, *44*, 1954−1958.
(60) De, S.; Chi, B.; Granier, T.; Qi, T.; Maurizot, V.; Huc, I. Designing Cooperatively Folded Abiotic Uni- and Multimolecular Helix Bundles. *Nat. Chem.* **2018**, *10*, 51−57.
(61) Lee, H.-J.; Ahn, I.-A.; Ro, S.; Choi, K. H.; Choi, Y.-S.; Lee, K.-B. Role of Aza Amino Acid Residue in Beta-Turn Formation and Stability in Designed Peptide. *J. Pept. Res.* **2000**, *56*, 35−46.
(62) Koch, O. Advances in the Prediction of Turn Structures in Peptides and Proteins. *Mol. Inf.* **2012**, *31*, 624−630.
(63) Wang, C. K.; King, G. J.; Northfield, S. E.; Ojeda, P. G.; Craik, D. J. Racemic and Quasi-Racemic X-ray Structures of Cyclic Disulfide-Rich Peptide Drug Scaffolds. *Angew. Chem., Int. Ed. Engl.* **2014**, *53*, 11236−11241.
(64) Handley, T. N. G.; Wang, C. K.; Harvey, P. J.; Lawrence, N.; Craik, D. J. Cyclotide Structures Revealed by NMR, with a Little Help from X-ray Crystallography. *ChemBioChem* **2020**, *21*, 3463−3475.
(65) Lin, R. B.; He, Y.; Li, P.; Wang, H.; Zhou, W.; Chen, B. Multifunctional Porous Hydrogen-Bonded Organic Framework Materials. *Chem. Soc. Rev.* **2019**, *48*, 1362−1389.
(66) Hisaki, I.; Xin, C.; Takahashi, K.; Nakamura, T. Designing Hydrogen-Bonded Organic Frameworks (HOFs) with Permanent Porosity. *Angew. Chem., Int. Ed.* **2019**, *58*, 11160−11170.
(67) Wang, B.; Lin, R.-B.; Zhang, Z.; Xiang, S.; Chen, B. Hydrogen-Bonded Organic Frameworks as a Tunable Platform for Functional Materials. *J. Am. Chem. Soc.* **2020**, *142*, 14399−14416.
(68) Busschaert, N.; Caltagirone, C.; Van Rossom, W.; Gale, P. A. Applications of Supramolecular Anion Recognition. *Chem. Rev.* **2015**, *115*, 8038−8155.
(69) Blažek Bregović, V.; Basarić, N.; Mlinarić-Majerski, K. Anion Binding with Urea and Thiourea Derivatives. *Coord. Chem. Rev.* **2015**, *295*, 80−124.
(70) Yuan, Y.; Yan, X.-S.; Li, X.-R.; Cao, J.-L.; Li, Z.; Jiang, Y.-B. Folded Short Azapeptide for Conformation Switching-based Fluorescence Sensing. *Chem. Commun.* **2017**, *53*, 13137−13140.
(71) Thordarson, P. Determining Association Constants from Titration Experiments in Supramolecular Chemistry. *Chem. Soc. Rev.* **2011**, *40*, 1305−1323.
(72) von Krbek, L. K. S.; Schalley, C. A.; Thordarson, P. Assessing Cooperativity in Supramolecular Systems. *Chem. Soc. Rev.* **2017**, *46*, 2622−2637.
(73) Kubik, S. Anion Recognition in Water. *Chem. Soc. Rev.* **2010**, *39*, 3648−3663.
(74) Ravikumar, I.; Ghosh, P. Recognition and Separation of Sulfate Anions. *Chem. Soc. Rev.* **2012**, *41*, 3077−3098.
(75) Moyer, B. A.; Custelcean, R.; Hay, B. P.; Sessler, J. L.; Bowman-James, K.; Day, V. W.; Kang, S. A Case for Molecular Recognition in Nuclear Separations: Sulfate Separation from Nuclear Wastes. *Inorg. Chem.* **2013**, *52*, 3473−3490.
(76) Smith, D. W. Ionic Hydration Enthalpies. *J. Chem. Educ.* **1977**, *54*, 540.
(77) Eller, L. R.; Stępień, M.; Fowler, C. J.; Lee, J. T.; Sessler, J. L.; Moyer, B. A. Octamethyl-octaundecylcyclo[8]pyrrole: A Promising Sulfate Anion Extractant. *J. Am. Chem. Soc.* **2007**, *129*, 11020−11021.
(78) Kim, S. K.; Lee, J.; Williams, N. J.; Lynch, V. M.; Hay, B. P.; Moyer, B. A.; Sessler, J. L. Bipyrrole-Strapped Calix[4]Pyrroles: Strong Anion Receptors that Extract the Sulfate Anion. *J. Am. Chem. Soc.* **2014**, *136*, 15079−15085.
(79) Qin, L.; Hartley, A.; Turner, P.; Elmes, R. B. P.; Jolliffe, K. A. Macrocyclic Squaramides: Anion Receptors with High Sulfate Binding Affinity and Selectivity in Aqueous Media. *Chem. Sci.* **2016**, *7*, 4563−4572.
(80) He, Q.; Kelliher, M.; Bähring, S.; Lynch, V. M.; Sessler, J. L. A Biscalix[4]pyrrole Enzyme Mimic That Constrains Two Oxoanions in Close Proximity. *J. Am. Chem. Soc.* **2017**, *139*, 7140−7143.
(81) Chen, S. Q.; Yu, S. N.; Zhao, W.; Liang, L.; Gong, Y. Y.; Yuan, L. F.; Tang, J.; Yang, X. J.; Wu, B. Recognition-Guided Sulfate Extraction and Transport Using Tripodal Hexaurea Receptors. *Inorg. Chem. Front.* **2022**, *9*, 6091−6101.

https://doi.org/10.1021/jacs.2c11684
J. Am. Chem. Soc. 2023, 145, 9530−9539